JAAS

ROYAL SOCIETY OF CHEMISTRY

PAPER

View Article Online
View Journal | View Issue

Cite this: J. Anal. At. Spectrom., 2025, 40, 3569

Development and investigation of efficient resonance ionization mass spectrometry schemes of gadolinium

Daniel Lauriola, * Michael Savina, Manuel Raiwa, Whitney Harmon and Brett Isselhardt

Received 22nd August 2025
Accepted 20th October 2025

DOI: 10.1039/d5ja00325c

rsc.li/jaas

Resonance ionization mass spectrometry of gadolinium can be used for nuclear forensics and to further the understanding of stellar nucleosynthesis but has been used only a handful of times due to the high laser power required and interference from non-resonant ionization of molecules of other elements. Herein we present the development of two novel resonance ionization spectroscopy schemes for gadolinium that provide improvements in isotopic fractionation and ionization efficiency, respectively, opening new applications for gadolinium analysis. The schemes are demonstrated and compared in a mixed sample of gadolinium and neodymium.

1. Introduction

Resonance ionization mass spectrometry (RIMS) has established itself as a powerful analytical technique due to its exceptional sensitivity and elemental selectivity.[1–4] Its applications span diverse fields including forensics, geology, and cosmochemistry, where it is routinely employed to determine isotopic compositions and elemental ratios critical for applications such as nuclear forensics,[5–9] tracing the origins of stardust grains,[10–12] and characterization of biomedical samples.[13] RIMS has been used for analysis of Xe, Zr, U, Pu, Ti, Fe, Cr, and many more elements.[14–23] For each element, efficient ionization pathways with minimal isotope shifts have been developed, enabling analysis with limited laser power and bandwidth.

Gadolinium (Gd) is of particular interest in nuclear forensics and presolar grain analysis due to its large neutron capture cross-section. Knowing the isotope ratios of Gd in extrasolar material such as stardust grains would increase our understanding of nucleosynthesis reactions in stars.[24] Determining trace concentrations of Gd is also essential in medicine for MRI contrast and targeted radiotherapy applications.[25–28]

However, only two resonance ionization schemes for Gd RIMS have been reported to date.[3,29] The first employs a three-laser scheme from a high-lying metastable state in the ground manifold ($J = 6$, $E = 1\,719$ cm^{-1}), populated at less than 10% below 1400 K,[29] limiting the measurement effectiveness to higher temperatures.[30] The second uses two colors and starts from the Gd ground state and has been successfully applied to clean samples.[3] Its use in complex materials is limited by the high fluences required to saturate the two-step process. Furthermore, the first transition of this scheme exhibits a large isotope shift, complicating the simultaneous measurement and comparison of all Gd isotopes and rendering the analysis sensitive to minor laser wavelength fluctuations. To overcome this, either the laser bandwidth needs to be broadened, leading to higher total fluence to maintain saturation, and increased oxide interferences, or a large correction factor could be applied for each isotope, lowering the accuracy, particularly in low concentration measurements, where RIMS is commonly used.

To address these limitations, we have developed and characterized two new ionization schemes for Gd RIMS, both using transitions from the $J = 3$, $E = 215$ cm^{-1} low-lying metastable state. We investigated a one-color, two-step pathway and a two-color scheme. The one-color scheme shows minimal isotope shifts but requires higher fluence, while the two-color scheme saturates at lower fluence and suppresses oxide interference more effectively. Here, we detail the characterization of these schemes, including isotope shifts, saturation fluences, and fractionation, and benchmark them on a mixed Gd/Nd sample to demonstrate improved performance in complex matrices.

2. Methods

2.1 RIMS instrument

All RIMS measurements were performed using the LION (laser ionization of neutrals) instrument at LLNL, which has been thoroughly described elsewhere,[7,11,19,31,32] and is briefly summarized here. The instrument consists of a vacuum chamber with ports for a desorption laser and ion guns for sputtering of the sample. Multiple tunable titanium sapphire (Ti : Sa) lasers can be coupled into the chamber through optical windows, to ionize the atoms of interest using multi-step ionization. A time-of-flight mass spectrometer determines the mass and counts of the ions

Lawrence Livermore National Laboratory, Nuclear and Chemical Sciences Division, 7000 East Ave, Livermore, CA, 94551, USA. E-mail: lauriola1@llnl.gov

produced by the laser interaction. For these specific experiments, Gd (and later Gd/Nd) was vaporized using a 1064 nm Nd:YVO_4 desorption laser running at 1.5 kHz. Each ~10 ns pulse is focused to ~75 μm and desorbs sub-monolayer quantities of material from the sample surface, shortly thereafter a high voltage pulse is applied to eject secondary ions produced by the desorption event. One microsecond later the multi-photon ionization laser pulses interact with the gas-phase Gd atoms in a ~1 mm^2 × ~3 mm long section to selectively ionize them. A 3 kV pulse then pushes the newly formed ions through a reflectron time-of-flight mass spectrometer, throughout which focusing and collimating optics direct them to the detector.

2.2 Lasers

The laser system has also been described elsewhere.[6,18,19] Four Ti : sapphire lasers were tuned to relevant wavelengths, and frequency doubled by LBO crystals to output ~15–20 ns, 0.1–0.5 mJ UV/visible pulses. We used four different lasers so that we could directly compare ionization schemes in real time. Two of the lasers were tuned to the reference scheme (Fig. 1) and run at a repetition rate of 750 Hz. The other two were pumped at 1500 Hz, with intra-cavity Q-switches to suppress every other pulse such that the Ti : Sa lasers operated at 750 Hz. Data was collected at 1500 Hz with the schemes interleaved such that the reference scheme was active during odd desorption laser shots and one of the new schemes shown in Fig. 1 was active during even shots. This makes it possible to benchmark to the reference pathway at every other pulse. The fundamental wavelength of each Ti : Sa was stabilized to within ±1.5 picometers using a closed feedback loop consisting of a wavemeter (WS6, High Finesse) and a piezo acting on the intracavity diffraction grating, with a 15 second update rate.

2.3 Samples

Two samples were used in the experiments. The first consisted of a 1 μL drop of 1000 ppm of natural gadolinium in 7% HNO_3 in an H_2O solution and deposited to cover ~2 mm of a clean Al substrate. Sample 2 consisted of a mix of a 1 μL droplet of the same Gd solution and 1 μL of a 1000 ppm of Nd 2% $HN0_3$ solution deposited on aluminum substrate, leading to a nominal mixture of 50 : 50 Gd/Nd by weight.

Before performing the measurements, the samples were imaged *in situ* using a microscope objective with ~5 μm resolution. The desorption laser was aligned to a uniform, particle free, area near the center of the dried droplet. The desorption laser was focused to ~75 μm to average out the effect of any possible μm sized particles or non-uniformities, not visible in the microscope images. The stage was moved to a new location whenever too much of the sample was depleted.

2.4 Spectroscopy

Saturation curves for each excitation step were determined by measuring the Gd ion count rate as a function of laser power. The signal level depends on both the ionization efficiency and the number of atoms desorbed by each laser shot. The use of a desorption laser to volatilize the sample leads to variations in the number of atoms desorbed from the sample and is susceptible to long-term power drift on the several minutes time scale. To account for this variation, saturation experiments were performed in reference to the signal from the 2-color ionization scheme previously published.[3] The use of a reference scheme on every other pulse allows for real time normalization of the data, which accounts for both the shot-to-shot and long-term variation in the material desorption rate.

For wavelength scans of the reference scheme (Fig. 2a), a different method was used, since there was no other pathway to compare to. Here a single scheme was used with the Ti : Sa lasers running at 1.5 kHz. An intracavity electro-optic deflector was placed in the first excitation step laser and used to deflect the beam hitting the grating to induce a small change in wavelength. The deflector was pulsed at 750 Hz, such that every other shot was at a fixed wavelength corresponding to the center of the excitation line while the application of varying voltages resulted in different wavelengths for the other shots. This allowed for changing the laser wavelength without energy or pointing variations. This enabled referencing, every other pulse, to the peak of the excitation line (no voltage applied) using the same ionization scheme, without requiring the use of two separate sets of lasers.

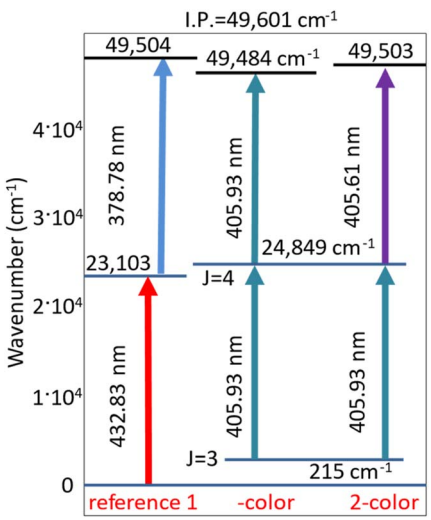

Fig. 1 Reference ionization pathway used (left) and newly developed schemes from the low-lying metastable state (center and right).

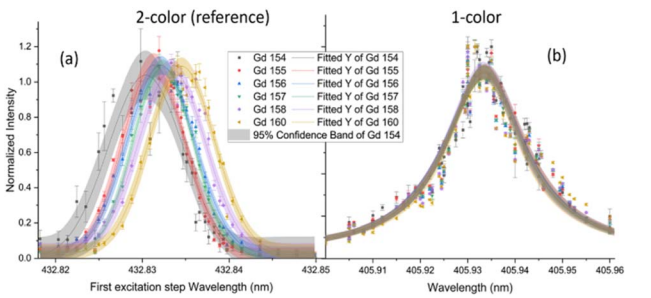

Fig. 2 Wavelength scans for (a) the 1st step of the reference two-color scheme and (b) the developed one-color scheme.

3. Results

3.1 Gadolinium resonance ionization schemes

Potential ionization schemes were identified from a comprehensive list of transitions.[33] Both the transitions from the $J = 3$ and from the $J = 5$ metastable states (215 cm^{-1} and 999 cm^{-1}) were investigated. Since the first metastable was more promising, the follow up characterization (Sections 3.3–3.6) was performed using the 215 cm^{-1} transition. Fig. 1 illustrates the previous ionization scheme (left), used as our reference, alongside the one-color and two-color schemes developed in this work; both starting from the $^9D^0$ $J = 3$ (215 cm^{-1}) metastable state.

Transitions from the $J = 5$ metastable state (999 cm^{-1}) were experimentally tested as well but are not presented here, as their ionization efficiency was approximately ten times lower; in line with an expected thermal population below ~10% at the estimated 700 K sample temperature.

3.2 Reference ionization pathway

The reference pathway (Fig. 1) we compared our new schemes to had already been published by others,[3] and had been previously used in our lab. For this work we also characterized the first excited state isotope shifts, as shown in Fig. 2a, and found a significant shift of 6 (±0.5) GHz from ^{154}Gd–^{160}Gd. The saturation fluences of this scheme were measured to be 0.5 mJ cm^{-2} and 17.5 mJ cm^{-2} respectively. The saturation curve of the second step is shown in Fig. 3.

3.3 One color ionization pathway

We performed wavelength scans to search for a 1-color photoionization pathway. A strong candidate was found at 405.933 nm. We assigned the first step to the known $\Delta J = +1$ transition from 215.124 cm^{-1} to 24 849.514 cm^{-1} (vacuum λ = 405.937 nm) as shown in Fig. 1 schematic. The second step, using the same laser wavelength, falls ~117 cm^{-1} below the ionization potential. (The electric field gradient in the LION instrument lowers the effective ionization potential of atoms by ~140 cm^{-1}.) Since it was not tabulated in literature and it is at a lower energy than experimental Rydberg scans performed by others,[34,35] we have not assigned it to any known transition. Wavelength scans for both the reference 2-color scheme, and the new 1-color transition are shown in Fig. 2. The reference scheme isotope shift is ~1 GHz per atomic mass unit. In the 1-color scheme the width of the peak scanned is nearly three times broader than the reference scheme. The isotope shifts are difficult to quantify due to the broad peak and the nearly perfect overlap in signal between different isotopes (Fig. 2b). Nevertheless, the ^{154}Gd–^{160}Gd shift is less than 0.75 GHz. Having an isotope shift that is >10× lower than the laser linewidth means that the isotopic ratios are less affected by changes in the laser wavelength and linewidth, which is ideal for isotopic analysis.

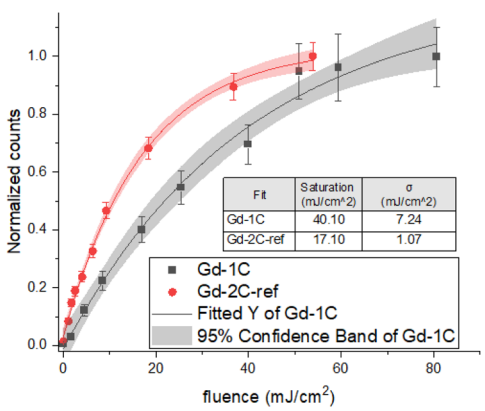

Fig. 3 Normalized saturation curve of the one-color scheme, and of the 2nd step of the reference scheme.

To determine the energy required to saturate the 1-color transition we adjusted the laser power with a half-wave plate/Glan laser polarizer combination. The maximum fluence for the 1-color pathway was 80 mJ cm^{-2}. Fitting the data in Fig. 3 was performed using a standard saturation fitting function[36] shown in eqn (1):

$$y = y_0 + y_{max} \times \left(1 - \exp\left(-\frac{x}{S}\right)\right) \quad (1)$$

where x is the fluence, y_{max} and y_0 represent the maximum ion counts, and background counts respectively; S is the value of the saturation fluence in mJ cm^{-2}.

For this transition we obtained a value of 40 (±7.2) mJ cm^{-2}, which is more than double the combined 17.5 mJ cm^{-2} saturation fluence of the reference scheme (0.4 mJ cm^{-2} for the first excited step, 17.1 mJ cm^{-2} for the 2nd excited step).

This new pathway has the advantages of a nearly absent isotope shift, which is beneficial for isotopic analysis, and requires only one laser. The drawback is that a high fluence is required, potentially increasing interference from non-resonant or quasi-resonant ionization molecules such as oxides in mixed samples.

To better understand why this ionization pathway requires such a high fluence, when the first excited level is a known resonant transition, we set out to characterize the second step transition.

We deployed a second laser at the same wavelength. We set the first laser to a fluence of 1.175 mJ cm^{-2} which yielded no Gd ionization but was enough to populate the 1st excited state. The second laser was then set to 6.4 mJ cm^{-2} and scanned over a range of more than 1 nm. The resulting scan, in Fig. 4, uncovered that the second photon of the one-color transition is only weakly coupled to the continuum, and multiple neighboring transitions to second excited states are much more efficient than that of the one-color scheme.

3.4 Two color ionization pathway

The discovery of the strong peak at 405.6 nm (Fig. 4) provides the basis for a potential two color ionization scheme. We first fixed one laser at 405.61 nm and scanned the first excited state laser from 405.907 to 405.965 nm in 2.5 pm steps. From the gaussian amplitude fits shown in Fig. 5a we determined a 9.75 (±0.87) GHz shift from ^{152}Gd to ^{160}Gd. We then set the first step laser to the peak, at 405.937 nm and scanned the second step

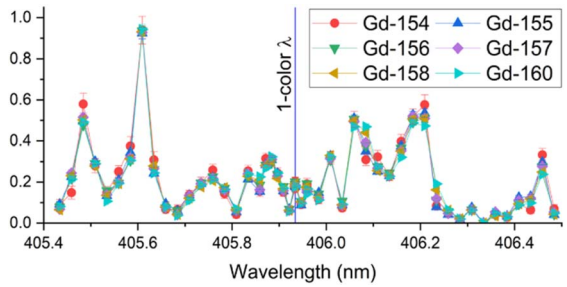

Fig. 4 Normalized wavelength scan of the second step laser to search for other upper state levels. The 1-color transition wavelength is shown by the blue vertical line.

from 405.560 to 405.650 nm. The second excited state presents a broader peak, overlapping a smaller secondary peak at +40 GHz, indicative of the high density of levels near the continuum. Fitting yields a total ^{152}Gd–^{160}Gd isotope shift of 6.86 (±1.19) GHz in the opposite direction of the first excited state. Determining the exact shifts and structure of these states would be interesting, but is beyond the scope of this work, and would require much narrower linewidth lasers.

These results show that both transitions have a significant isotope shift, in opposite directions. The first step has ∼1.2 GHz per amu for the even isotopes, and the second step shift is ∼−0.8 GHz per amu in the other direction. Since the isotope shifts are opposite, and the lasers linewidths are broad, we found that in our experiments, using saturated laser fluences, setting the 1st and 2nd excited state lasers to 405.937 nm and 405.611 nm, respectively, resulted in an isotope fractionation of <5%. This is explained by a higher excitation probability of the heavier isotopes in the first transition, followed by a higher excitation probability of the lighter ones in the second transition, due to the opposite shift. Since the shifts are not identical and opposite, and there is more structure in the second excited

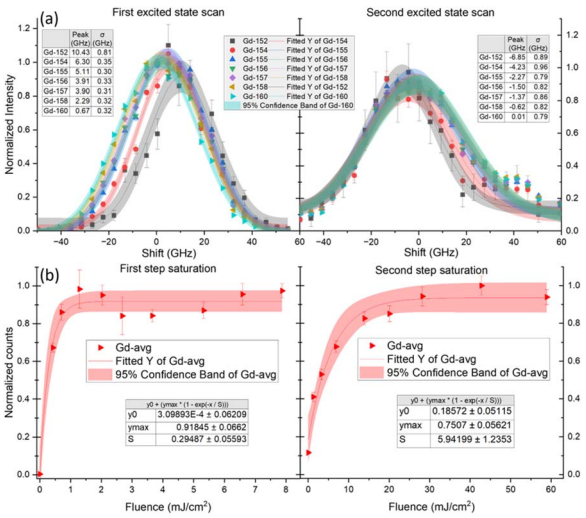

Fig. 5 (a) First and second excited state wavelength scans to determine the isotope shifts; (b) saturation curves for the first and second excited state levels.

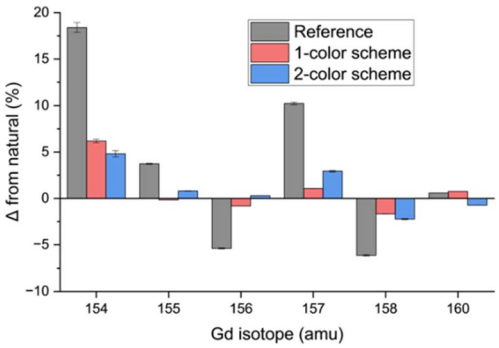

Fig. 6 Isotope fractionation compared to the natural abundance of Gd for the schemes used. Results are obtained from measurements above the saturation fluence.

state, we don't expect an exact compensation of the two, as is reflected by the residual non-zero fractionation in Fig. 6.

We scanned the laser energy for both transitions and fit the curves using the fitting function defined by eqn (1). The results in Fig. 5b show that both steps saturate at very low fluences. The first shows a saturation fluence of 0.29 mJ cm^{-2}. The second step saturates at ∼6 mJ cm^{-2}, 3 times lower than the reference scheme (17.1 mJ cm^{-2} saturation).

3.5 Scheme comparisons

Table 1 shows a summary of the main characteristics of the three schemes under study. The data for the reference scheme was also taken in our laboratory under the same conditions. We did not measure the isotope shifts of the second excited state of the reference scheme.

Comparing these schemes we find that the main advantage of the 1-color scheme is the broad excitation peak and near absence of isotope shifts, making it more insensitive to variations in laser linewidth and power; while a high fluence is required to saturate the transition, since the second step does not appear to be coupled to a strongly resonant level. The new two-color scheme has similar isotope shifts as the reference scheme, but the saturation energy is ∼3 times lower, placing it at a strong advantage for mixed samples.

Additional measurements of the isotope fractions (Fig. 6) showed that the reference two-color scheme favors the odd isotopes over the even ones due to selection rules and shows more fractionation of ^{154}Gd due to a narrower linewidth. The new schemes both have much lower fractionation than the reference scheme, which is nearly 20%. The 1-color scheme

Table 1 Summary of the resonance ionization schemes

	Reference	1-Color	2-Color
Step 1 (nm)	432.832	405.933	405.937
Step 2 (nm)	378.78		405.611
Sat 1 (mJ cm^{-2})	0.5	40	0.29
Sat 2 (mJ cm^{-2})	17.5		5.94
Relative signal	1	0.6	1.5
Isotope shift (GHz per amu)	1; N/A	<0.1	+1.2;-0.8

presents a maximal change from natural of 7% for ^{154}Gd but is the closest to natural composition overall. The 2-color scheme differs by <5% for ^{154}G but does show more variation in the ratio between even and odd isotopes. Lower fractionation can improve sensitivity by requiring a smaller correction when using a standard in measurements. Use of standard-sample-standard bracketing can correct for similar amount of fractionation, and is used in all mass spectrometry measurements, including RIMS.

3.6 Demonstration on a mixed Gd/Nd sample

A major limitation for Gd-RIMS is isobaric interference from molecules of other elements, whose masses may overlap with one or more of the Gd isotopes. Neodymium oxides are of particular concern due to ^{142}Nd^{16}O interference with ^{158}Gd and ^{144}Nd^{16}O interference with ^{160}Gd.

To evaluate the selectivity of each pathway on a complex sample, we performed experiments on a sample with 1000 ppm of Gd and 1000 ppm of Nd. Fig. 7 shows two mass spectra taken in the previously described interleaving mode over a 5 minute-long acquisition. There are no interfering molecules from mass 154 to 157 and the Gd signals are comparable for both schemes, however the signals above mass 158 are significantly different due to NdO interference. The Gd-free peaks at 159 amu and 161 amu can be used as a direct comparison for the number of interfering oxides ionized. Higher interference of NdO within the Gd peaks increases the difficulty in obtaining isotopic ratios. Some corrections can be made, and an interleaved blinking scheme to compare off-resonance spectra and subtract the oxide counts, could be applied, but the uncertainty would still be increased. This solution would be especially challenging if counts per run are extremely low, and where ^{158}Gd and ^{160}Gd, due to their higher natural abundance, may be the only isotopes well above the detection limit.

As in the previous experiments, the new pathways were compared to the reference 2-color scheme which was interleaved at each shot. We set the reference scheme first and second excited step fluences to 1.17 mJ cm^{-2} and 87 mJ cm^{-2} respectively to ensure complete saturation and varied the 1-color and two-color scheme fluences to study the effect on signal and oxide interference. The fluence of the first step of the newly developed 2-color scheme was fixed at 1.5 mJ cm^{-2}, far above its 0.3 mJ cm^{-2} saturation value.

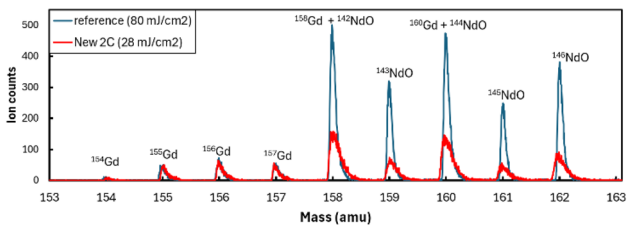

Fig. 7 Raw mass spectra of Gd/Nd sample during one run, highlighting areas of overlap between Gd and Nd oxides. The two spectra have similar Gd signal, but the reference scheme ionized much more Nd oxide.

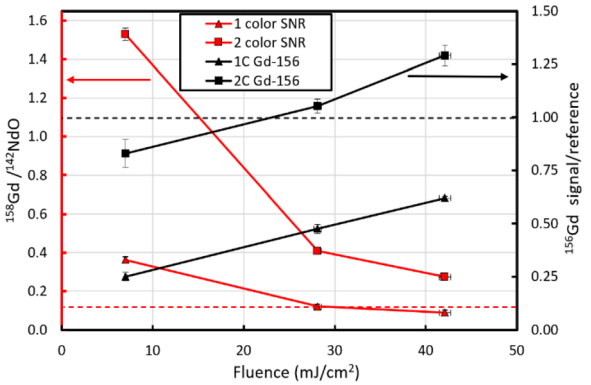

Fig. 8 Signal and NdO interference as a function of fluence for the new schemes relative to the reference. Right axis (black): ^{156}Gd signal. Left axis (red): The ratio of resonantly ionized Gd to non-resonantly ionized NdO. Dashed lines represent the reference scheme, which was set far above saturation (87 mJ cm^{-2}). For the 2-color schemes the *x*-axis refers to fluence of the second excited step laser.

We used ^{156}Gd to compare the signal at different fluences as it is the most abundant interference-free isotope. The ratio of the integrated areas of ^{156}Gd of the new schemes to the reference is shown on the right axis in Fig. 8. On the left axis we plotted the signal to oxide ratio at the ^{158}Gd peak, for the new schemes; this is obtained by first calculating the expected ^{158}Gd signal from the ^{154}Gd to ^{157}Gd peaks and the known isotopic ratio obtained from the pure Gd sample. The remaining signal, after subtracting ^{158}Gd, is assigned to ^{142}NdO. The highest ^{158}Gd/^{142}NdO ratio is 1.53 using the new two-color scheme at 7 mJ cm^{-2}; compared to a ratio of 0.15 (red dotted line) for the reference scheme at the high 87 mJ cm^{-2} fluence.

The results in Fig. 8 show that in terms of oxide interference the one-color scheme performs worse than the reference 2-color scheme. At the highest fluence the signal is 0.6 times that of the reference, and the Gd/NdO ratio is also 20% lower than the reference scheme. The newly developed 2-color scheme is much better; at the highest fluence the signal is 1.3 times higher, and the Gd/NdO ratio is 1.8 times better than the reference. At 7 mJ cm^{-2} where the signal is nearly comparable to the reference (~17% less) the oxide interference is suppressed by a factor of ~14.5, providing a significant advantage in mixed sample measurements. If performing measurements far above saturation is essential, running at ~20–25 mJ cm^{-2} would result in similar efficiencies to the reference scheme, while reducing the oxide interference by a factor of ~5–8.

3.7 Temperature independence of the new pathways

An additional advantage of the new schemes is that efficiency is expected to be nearly constant across a broad range of temperatures. Using the assumption that *J* levels in the same manifold follow a Boltzmann distribution, as if they were in thermal equilibrium, we calculated the population distributions of the ground state manifold of Gd from the partition function and NIST data[37] and plotted them in Fig. 9. While the temperature of the vapor plume was not measured, we note that

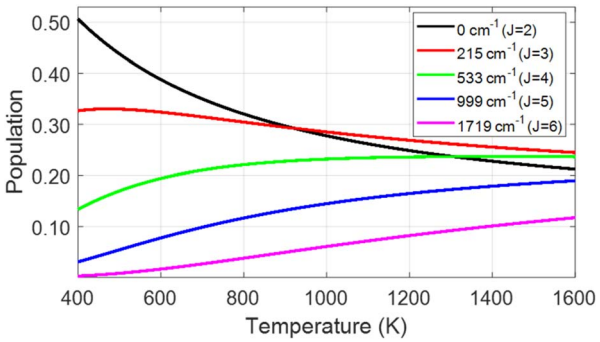

Fig. 9 Calculated population distribution of the levels in the ground state manifold of gadolinium as a function of temperatures.

previous work in the LION instrument measuring the metastable ratios of atoms resulted in temperatures below 1000 K.[17] While the ground state depopulates significantly with temperature, the $J = 3$ population is nearly constant, remaining between 0.28 and 0.32 over the range from 400 to 1000 K. This shows that throughout a broad range of temperatures, using this scheme from the first metastable level will result in a lower temperature dependence compared to the ground level. It should be noted that due to the low number of atoms desorbed, this measurement occurs in a virtually collision free environment. In this environment the states shown in Fig. 9, which are in the same $^9D^0$ manifold follow a Boltzmann distribution, but other levels will not be in thermal equilibrium.

4. Conclusions

We have developed two new RIMS schemes for isotopic analysis of gadolinium, both of which originate on the first metastable state. The first pathway is a one-color, two-photon excitation scheme with very low isotope shifts and hence isotopic fractionation and requires only a single laser, however it requires a relatively high saturation fluence. The second is a two-color scheme with significantly lower saturation fluences than either the one-color or the reference two-color RIMS schemes. We applied the new schemes to a sample with 50% Nd and benchmarked the results to the reference Gd pathway. The results show a factor of ~10 improvement in oxide suppression at equal signal using the newly developed two-color scheme. Future development could include broader upper state scans to find higher cross-section Rydberg states close to the continuum and further reduce the laser fluence required, as well as applications of the newly developed pathways to relevant samples.

Author contributions

Daniel L.: conceptualization, data curation, formal analysis, investigation, methodology, visualization, writing – original draft preparation; Michael S.: conceptualization, resources, supervision, writing – review & editing (identified the potential transitions to explore and consulted on the path forward throughout); Manuel R.: investigation, methodology (laser tuning and alignment, guidance on running the LION instrument, and wavelength scans) Whitney H.: investigation, methodology (wavelength, saturation, and mixed sample scans). Brett I.: funding acquisition, methodology, project administration, writing – review & editing. All authors have read and agreed to the published version of this manuscript.

Conflicts of interest

There are no conflicts to declare.

Data availability

The data supporting this article have been included as part of the supplementary information (SI). Supplementary information is available. See DOI: **https://doi.org/10.1039/d5ja00325c**.

Acknowledgements

The authors would like to thank Danielle Ziva Shulaker for providing the samples used in this work, and Mark Rotter for insights on the metastable state populations of Gadolinium. This work was performed under the auspices of the U.S. Department of Energy by Lawrence Livermore National Laboratory under Contract DE-AC52-07NA27344. LLNL-JRNL-2007314. This work was supported by the Laboratory Directed Research and Development Program at LLNL under project 25-ERD-011.

Notes and references

1 D. H. Smith, D. L. Donohue and J. P. Young, Determination of isotopic ratios of neodymium by resonance ionization mass spectrometry, *Int. J. Mass Spectrom. Ion Processes*, 1985, **65**(3), 287–297.
2 D. L. Donohue, J. P. Young and D. H. Smith, Resonance ionization photoelectron spectroscopy of lanthanide elements, *J. Chem. Phys.*, 1986, **85**(9), 4794–4801.
3 A. Ofan, I. Ahmad, J. P. Greene, M. Paul and M. R. Savina, Development of a detection method for 244Pu by Resonance Ionization Mass Spectrometry, *New Astron. Rev.*, 2006, **50**(7–8), 640–643.
4 J. Levine, M. R. Savina, T. Stephan, *et al.*, Resonance ionization mass spectrometry for precise measurements of isotope ratios, *Int. J. Mass Spectrom.*, 2009, **288**(1), 36–43.
5 H. Bosco, L. Hamann, N. Kneip, *et al.*, New horizons in microparticle forensics: Actinide imaging and detection of ^{238}Pu and ^{242m}Am in hot particles, *Sci. Adv.*, 2021, **7**(44), eabj1175.
6 M. R. Savina, B. H. Isselhardt, D. Shulaker, M. Robel, A. Conant and B. J. Ade, Simultaneous determination of Sr, Mo, and Ru relative isotope abundances by resonance ionization mass spectrometry of fission products in spent nuclear fuel particles, *Sci. Rep.*, 2023, **13**, 5193.
7 M. R. Savina, B. H. Isselhardt and R. Trappitsch, Simultaneous isotopic analysis of U, Pu, and Am in spent

nuclear fuel by resonance ionization mass spectrometry, *Anal. Chem.*, 2021, **93**(27), 9505–9512.

8 M. Raiwa, M. R. Savina, A. G. Roberts, D. Z. Shulaker and B. H. Isselhardt, Actinide Elemental Ratios of Spent Nuclear Fuel Samples by Resonance Ionization Mass Spectrometry, *J. Am. Soc. Mass Spectrom.*, 2024, **35**(12), 3233–3241.

9 M. Raiwa, S. Büchner, N. Kneip, *et al.*, Actinide imaging in environmental hot particles from Chernobyl by rapid spatially resolved resonant laser secondary neutral mass spectrometry, *Spectrochim. Acta, Part B*, 2022, 106377.

10 N. Liu, M. R. Savina, A. M. Davis, *et al.*, Development of a Resonance Ionization Method for Isotopic Analysis of Neodymium at Trace Levels in Presolar SiC Grains, *43rd Annual Lunar and Planetary Science Conference*, The Woodlands, Texas, 2012.

11 R. Trappitsch, W.-J. Ong, C. J. Dory, *et al.*, Simultaneous Analyses of Titanium and Molybdenum Isotopic Compositions in Presolar SiC Grains, *Paper Presented at: 84th Annual Meeting of the Meteoritical Society*, 2021.

12 I. Pal, M. Jadhav, D. Z. Shulaker, M. R. Savina Heavy Element Isotopic Analysis of Low Density Graphite Grains with LION, *Paper Presented at: 54th Lunar and Planetary Science Conference*, The Woodlands, Texas, 2023.

13 K. Wendt, K. Blaum, B. A. Bushaw, *et al.*, Recent developments in and applications of resonance ionization mass spectrometry, *Fresenius. J. Anal. Chem.*, 1999, **364**(5), 471–477.

14 S. A. Crowther, R. K. Mohapatra, G. Turner, D. J. Blagburn, K. Kehm and J. D. Gilmour, Characteristics and applications of RELAX, an ultrasensitive resonance ionization mass spectrometer for xenon, *J. Anal. At. Spectrom.*, 2008, **23**(7), 938–947.

15 R. Trappitsch, D. Shulaker, W.-J. Ong, M. Savina and B. Isselhardt, Resonance ionization of zirconium, *J. Radioanal. Nucl. Chem.*, 2022, **331**(12), 5199–5204.

16 S. Raeder, V. Sonnenschein, T. Gottwald, *et al.*, Resonance ionization spectroscopy of thorium isotopes–towards a laser spectroscopic identification of the low-lying 7.6 eV isomer of229Th, *J. Phys. B: At., Mol. Opt. Phys.*, 2011, **44**(16), 165005.

17 R. Trappitsch, M. R. Savina and B. H. Isselhardt, Resonance ionization of titanium: high useful yield and new autoionizing states, *J. Anal. At. Spectrom.*, 2018, **33**(11), 1962–1969.

18 M. R. Savina, B. H. Isselhardt, A. Kucher, *et al.*, High useful yield and isotopic analysis of uranium by resonance ionization mass spectrometry, *Anal. Chem.*, 2017, **89**(11), 6224–6231.

19 B. Isselhardt, M. Savina, A. Kucher, S. Gates, K. Knight and I. Hutcheon, Improved precision and accuracy in quantifying plutonium isotope ratios by RIMS, *J. Radioanal. Nucl. Chem.*, 2016, **307**, 2487–2494.

20 C. Gruning, G. Huber, P. Klopp, *et al.*, Resonance ionization mass spectrometry for ultratrace analysis of plutonium with a new solid state laser system, *Int. J. Mass Spectrom.*, 2004, **235**(2), 171.

21 P. G. Schumann, K. D. A. Wendt and B. A. Bushaw, High-resolution triple-resonance autoionization of uranium isotopes, *Spectrochim. Acta, Part B*, 2005, **60**(11), 1402–1411.

22 N. Kneip, C. E. Düllmann, V. Gadelshin, *et al.*, Highly selective two-step laser ionization schemes for the analysis of actinide mixtures, *Hyperfine Interact.*, 2020, **241**(1), 45.

23 M. Miyabe, Y. Iwata, H. Tomita, M. Morita and T. Sakamoto, Resonance ionization spectroscopy of neodymium for determining a highly efficient two-step ionization scheme, *Spectrochim. Acta, Part B*, 2024, **221**, 107036.

24 A. Mazzone, S. Cristallo, O. Aberle, *et al.*, Measurement of the 154Gd(n,γ) cross section and its astrophysical implications, *Phys. Lett. B*, 2020, **804**, 135405.

25 G. Famulari, T. Urlich, A. Armstrong and S. A. Enger, Practical aspects of 153Gd as a radioactive source for use in brachytherapy, *Appl. Radiat. Isot.*, 2017, **130**, 131–139.

26 S. A. Enger, D. R. Fisher and R. T. Flynn, Gadolinium-153 as a brachytherapy isotope, *Phys. Med. Biol.*, 2013, **58**(4), 957.

27 L. Xie, J. Qin, C. Song, *et al.*, 157Gd-DOTA-PSMA as theranostic bio-gadolinium agent for prostate cancer targeted gadolinium neutron capture therapy, *J. Cancer Res. Clin. Oncol.*, 2025, **151**(2), 93.

28 K. Blaum, C. Geppert, W. Schreiber, *et al.*, Trace determination of gadolinium in biomedical samples by diode laser-based multi-step resonance ionization mass spectrometry, *Anal. Bioanal. Chem.*, 2002, **372**(7), 759–765.

29 K. Blaum, B. A. Bushaw, W. Nörtershäuser and K. Wendt, High-resolution, three-step resonance ionization mass spectrometry of gadolinium, *AIP Conf. Proc.*, 2001, **584**(1), 141–144.

30 C. Geppert, K. Blaum, S. Diel, P. Müller, W. G. Schreiber and K. Wendt, Gadolinium trace determination in biomedical samples by diode-laser-based multi-step resonance ionization mass spectrometry, *AIP Conf. Proc.*, 2001, **584**(1), 249–254.

31 D. Z. Shulaker, R. Trappitsch, M. R. Savina and B. Isselhardt, High-useful yield and new autoionizing state of resonantly ionized tungsten, *J. Anal. At. Spectrom.*, 2023, **38**(2), 457–463.

32 B. Isselhardt, M. Savina, K. Knight, M. Pellin, I. Hutcheon and S. Prussin, Improving precision in resonance ionization mass spectrometry: influence of laser bandwidth in uranium isotope ratio measurements, *Anal. Chem.*, 2011, **83**(7), 2469–2475.

33 J. E. Sansonetti and W. C. Martin, Handbook of Basic Atomic Spectroscopic Data, *J. Phys. Chem. Ref. Data*, 2005, **34**(4), 1559–2259.

34 B. A. Bushaw, W. Nörtershäuser, K. Blaum and K. Wendt, Studies of narrow autoionizing resonances in gadolinium, *Spectrochim. Acta, Part B*, 2003, **58**(6), 1083–1095.

35 M. Miyabe, M. Oba and I. Wakaida, Analysis of the even-parity Rydberg series of Gd I to determine its ionization potential and isotope shift, *J. Phys. B: At., Mol. Opt. Phys.*, 1998, **31**(20), 4559.

36 V. Letokhov, *Laser Photoionization Spectroscopy*, Elsevier, 2012.

37 A. Kramida, Y. Raichenko, and J. Reader, *NIST Atomic Spectra Database v 5.12*, Technology NioSa, 2024.